iScience

Article

Coal fly ash-derived zeolite for efficient ammoniacal nitrogen removal from freshwater pearl farming wastewater

Graphical abstract

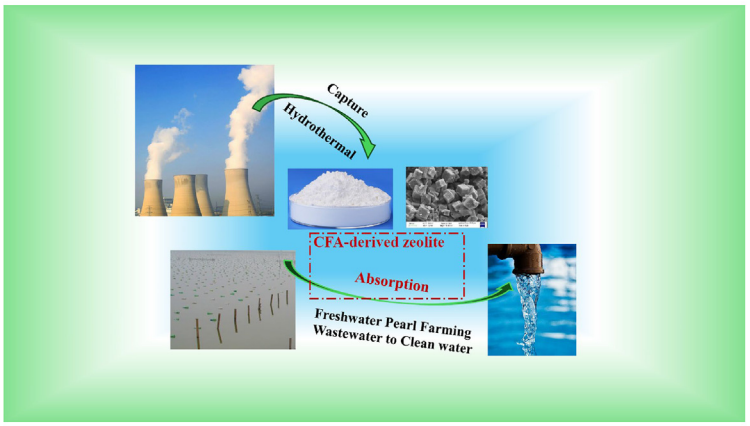

Authors

Bo Xia, Honghao Chen, Juntao Wang, Xiaocheng Pan

Correspondence

11106142@zju.edu.cn (B.X.), panxiaocheng1210@163.com (X.P.)

In brief

Environmental chemistry; Environmental management; Aquatic science

Highlights

- Efficient strategy to mitigate overfeeding-induced environmental threats in pearl farming
- Utilizing coal fly ash as a valuable resource enhances environmental sustainability
- Achieving a win-win between traditional industries and the emerging aquaculture industry

Xia et al., 2025, iScience *28*, 111645
January 17, 2025
https://doi.org/10.1016/j.isci.2024.111645

CellPress

iScience

CellPress
OPEN ACCESS

Article

Coal fly ash-derived zeolite for efficient ammoniacal nitrogen removal from freshwater pearl farming wastewater

Bo Xia,[1,2,3,*] Honghao Chen,[1,2] Juntao Wang,[1] and Xiaocheng Pan[1,*]
[1]Department of Biological Environment, Jiyang College of Zhejiang A&F University, Zhuji, China
[2]These authors contributed equally
[3]Lead contact
*Correspondence: 11106142@zju.edu.cn (B.X.), panxiaocheng1210@163.com (X.P.)
https://doi.org/10.1016/j.isci.2024.111645

SUMMARY

Freshwater pearl farming in China generates wastewater high in ammoniacal nitrogen (NH_3-N) posing environmental threats. This study explores the use of coal fly ash (CFA), an industrial waste, to synthesize A-type zeolite for effective NH_3-N removal from pearl farming wastewater. The zeolite was prepared via pickling pretreatment and hydrothermal methods, resulting in a material with favorable adsorption properties, including cubic and spherical microstructures, a specific surface area of 17.5 m^2/g, an average pore size of 10.7 nm, and a pore volume of 0.03 cm^3/g. Adsorption experiments showed that NH_3-N removal followed *pseudo-first-order* kinetics and fit the *Dubinin-Radushkevich* isotherm model. Applied to actual wastewater, the zeolite achieved a 74% removal efficiency at a dosage of 70 g/L. This approach converts CFA into a valuable adsorbent, reducing its environmental impact, and enhances the sustainability of freshwater pearl farming through effective wastewater treatment, and demonstrates the potential of transforming industrial waste into functional materials for environmental remediation.

INTRODUCTION

Pearls, whether sourced from seawater or freshwater, have long been esteemed as symbols of jewelry in China, a tradition that spans thousands of years. Statistics indicate that China's pearl industry reached a valuation of $11.4 billion in 2023. As pearls continue to gain favor among consumers, pearl farming has emerged as a pillar industry for numerous local governments in China. Compared to the 2.3 metric tons of seawater pearl production, freshwater pearl farming significantly dominates, with an output of 697 metric tons. However, to boost pearl production, overfeeding pearl oysters is common, leading to wastewater with high ammoniacal nitrogen (NH_3-N) content, which poses a serious threat to the local environment.[1,2] Thus, finding an efficient method for removing NH_3-N from freshwater pearl farming wastewater holds substantial economic value. Various strategies for NH_3-N removal, including membrane separation, ion exchange, chemical precipitation, and microbiological methods, have been explored.[3,4] However, these methods often encounter challenges such as high costs, complex operations, limited applicability to high concentrations, or low microorganism survival rates in practical applications.[5] To address these limitations, adsorption using adsorbents has gained traction among researchers as a quick, simple, and effective method.[6–15]

In recent years, synthesized zeolite derived from coal fly ash (CFA) has shown exceptional performance in the field of adsorption.[16–22] As a primary by-product of coal combustion, CFA predominantly contains silicon dioxide (SiO_2) and aluminum oxide (Al_2O_3) and possesses a porous structure like that of naturally occurring zeolites.[18,19] These compositions make CFA a promising and cost-effective material for zeolite synthesis. The potential of CFA-derived zeolite has been widely recognized across various environmental applications, proving particularly effective in atmospheric and soil remediation.[16,23,24] In wastewater treatment, CFA-derived zeolite has distinguished itself as an efficient adsorbent, successfully separating oil from wastewater[25] and absorbing heavy metal ions, thereby significantly reducing the concentrations of toxic metals and preventing their harmful effects on aquatic ecosystems and human health.[26] Moreover, it has demonstrated efficacy in decreasing levels of phosphorus, chemical oxygen demand (COD), and NH_3-N in industrial wastewater-reductions that are vital for preventing eutrophication in aquatic environments and for ensuring compliance with stringent environmental regulations.[17,27–29] Given its high performance and cost-effectiveness, CFA-derived zeolite continues to garner attention as a versatile and valuable material for a wide range of environmental remediation applications.

In this study, CFA-derived zeolite was evaluated as an efficient adsorbent for removing NH_3-N from freshwater pearl farming wastewater (Figure 1). The zeolites were synthesized from acid-treated fly ash, and the effects of preparation parameters on ammonium adsorption were investigated. Several advanced analytical techniques, including X-ray diffraction (XRD), Brunauer-Emmett-Teller (BET) surface analysis, energy dispersive

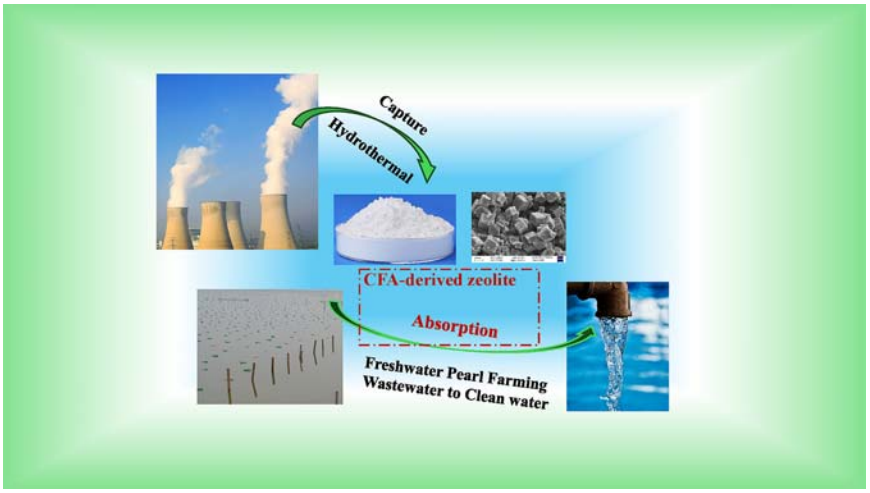

Figure 1. Schematics of CFA-derived zeolite for removing NH_3-N from freshwater pearl farming wastewater

spectroscopy (EDS), scanning electron microscopy (SEM), and transmission electron microscopy (TEM), were employed to gain valuable insights into the zeolite's characteristics. By assessing the physicochemical properties of the raw materials alongside the pretreatment and synthesis methods, our research focused on treating ammonium-rich wastewater using these synthetic products. The adsorption behavior and mechanisms were examined under various conditions, including pH value, initial ammonium concentration, temperature, adsorbent dosage, and the presence of coexisting ions. Additionally, the application of the synthesized zeolite for ammonium adsorption from real freshwater pearl farming wastewater was evaluated. In summary, this study successfully demonstrates the immense efficacy of CFA-derived zeolite for the removal of NH_3-N from freshwater pearl farming wastewater.

RESULTS AND DISCUSSIONS

Optimization for CFA-derived zeolite synthesis

Since the CFA was directly obtained from a local thermal power plant, it required purification to increase the content of Si and Al. According to the literature, the main metallic oxides that influence zeolite preparation are Fe_2O_3, CaO, and MgO, which can be removed through pickling.[30] Therefore, diluting hydrochloric acid was applied, and various concentrations were investigated. Results, shown in Figure 2A., indicated that as the concentration of dilute hydrochloric acid increased, the mass loss percentage changed significantly. At a concentration of 5%, the CFA lost 7.5% of its weight. Further increases in concentration from 5% to 15% did not yield better results. Considering that excessive hydrochloric acid can also cause the loss of SiO_2 and Al_2O_3, a 5% concentration was selected for further optimization. After determining the appropriate concentration of dilute hydrochloric acid, the influence of factors such as temperature, the ratio of CFA to HCl, reaction time, and screen number were investigated. These results are presented in Figures 2B–2E. The optimal conditions were determined to be a 200-mesh screen and a 15% weight ratio of dilute hydrochloric acid, achieving the best results with a 2-h pickling process at 85°C. XRF testing indicated that the percentages of SiO_2 and Al_2O_3 increased from 48.2% to 33.2%–51.8% and 37.6%, respectively (Figure 2F). Concurrently, the percentages of Fe_2O_3 and CaO decreased to 3.2% and 5.7%. Additionally, the content of TiO_2 and MgO decreased significantly.

With the purified CFA obtained, hydrothermal synthesis was employed to prepare CFA-derived zeolite. As shown in Figure 3A, the dosage of NaOH plays a crucial role in NH_3-N adsorption efficiency. Increasing the ratio of CFA/NaOH (w/w) from 0.5 to 1.2 resulted in a significant improvement in NH_3-N removal efficiency, raising it from 32% to 68%. However, further increasing the NaOH dosage did not yield better results; the NH_3-N removal efficiency began to decrease when the ratio reached 1.4. The highest NH_3-N removal efficiency of 81.6% was observed at a hydrothermal synthesis temperature of 85°C (Figure 3B). Conversely, when the synthesis temperature was increased to 95°C, the NH_3-N removal efficiency decreased to 71.6%. The influence of synthesis time revealed a continuous decreasing trend (Figure 3C). Initially, a 6-h hydrothermal synthesis achieved an NH_3-N removal efficiency of 81.6%. However, when the synthesis time was extended to 24 h, the removal efficiency dropped to 61.1%. We believe that high temperatures and prolonged synthesis times may cause the material to clump, thereby decreasing the specific surface area of the zeolite.[31] Consequently, the removal efficiency changes significantly.

Characterization of CFA-derived zeolite

XRD was employed to analyze the crystalline phases of the synthetic CFA-derived zeolite, with its diffraction patterns displayed in Figure 4. The results reveal notably strong diffraction peaks characteristic of type A zeolite, prominently and sharply observed at 7.2°, 10.1°, 12.4°, 16°, 21.6°, 23.9°, 27°, 29.8°, 32.5°, and 34.1°, which points to its high crystallinity.[32–34] These sharp peaks not only signify a well-defined crystalline structure but also confirm that type A zeolite is the predominant product formed during the synthesis process. The high intensity and clarity of these peaks indicate that the synthesized zeolite possesses an ordered and homogeneous framework, essential for its effectiveness in applications like adsorption and ion exchange. Among the predominant A-type zeolite synthesized, the XRD patterns also revealed the presence of a small quantity of X-type zeolite, as indicated by characteristic peaks at 20.3°, 23°, 30.7°, and 33.3°.[35] The detection of these peaks suggests that, although type A zeolite is the main product, the synthesis conditions also favored the formation of X-type zeolite to a minor extent. Overall, the XRD analysis underscores the successful

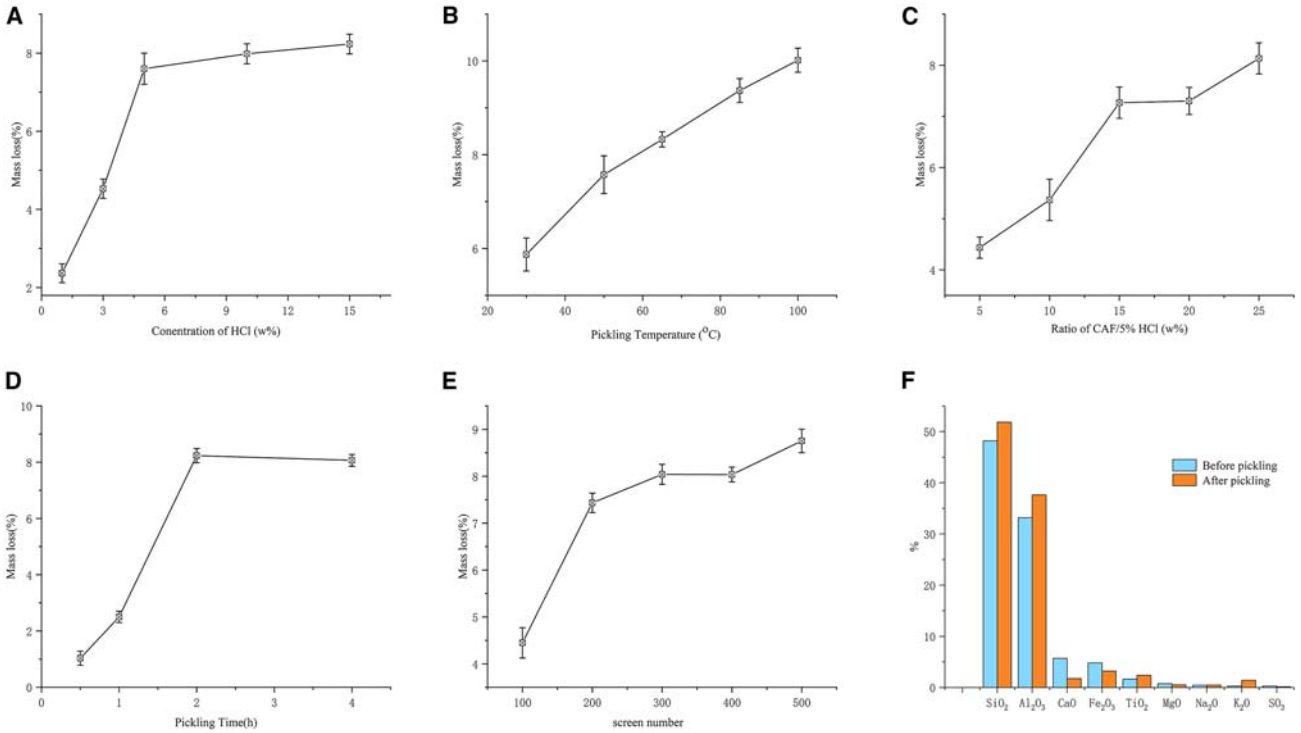

Figure 2. Optimization of pretreatment parameters

Optimization of pretreatment parameters, data are represented as mean ± SEM: (A) concentration of HCl; (B) pickling temperature; (C) ratio of CFA/5% HCl; (D) pickling time; (E) screen number and (F) component comparison before and after pickling.

synthesis of high-crystallinity type A zeolite with a small amount of X-type zeolite.

Figure 5A presents the SEM image of the CFA-derived zeolite, providing a detailed visualization of its microstructure. As depicted in the figure, two distinct types of crystals can be observed: cubic crystals and spherical crystals with intersecting surfaces, both exhibiting regularly defined shapes. This observation is corroborated by TEM imaging shown in Figure 5B, further confirming the presence of these crystal structures. The cubic crystal structure can be further classified into two subtypes based on their size. The first subtype consists of small cubic crystals, with a particle size of approximately 0.6 μm. These

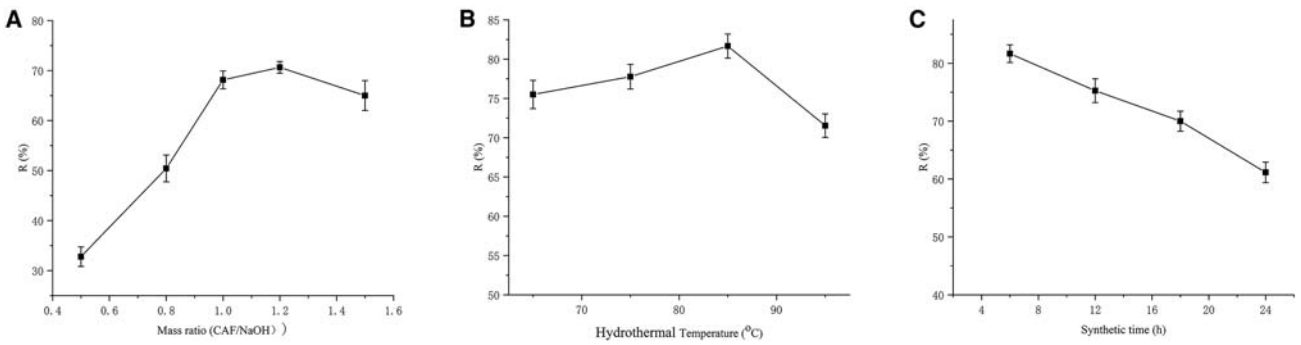

Figure 3. Optimization of synthetic parameters for CFA-derived zeolite

Synthetic parameters of CFA-derived zeolite, data are represented as mean ± SEM: (A) CFA/NaOH (w/w); (B) hydrothermal temperature; (C) synthetic time (C_0 = 100 mg/L; adsorbent dosage = 5 g/L; pH = 7.0; T = 25°C).

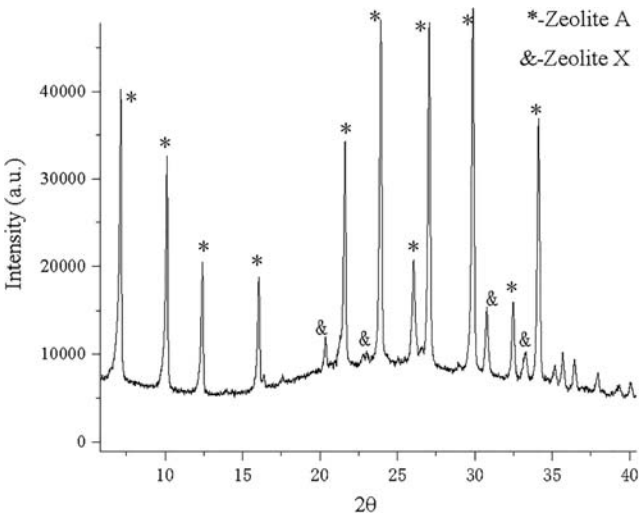

Figure 4. XRD of synthetic CFA-derived zeolite: *-zeolite A, and -zeolite X

smaller cubic particles contribute to the overall texture and surface area of the zeolite. The second subtype includes larger cubic crystals, with a particle size of around 1.5 μm, which provide additional structural stability and may affect the material's mechanical properties. Meanwhile, the spherical crystal particles have a uniform size of about 1.0 μm. These spherical particles add diversity to crystal morphology and possibly influence the porosity and adsorption characteristics of zeolite. Additionally, it's important to note that the surface of the CFA-derived zeolite crystals is accompanied by amorphous impurities. These amorphous regions may result from incomplete crystallization or residual materials from the synthesis process. The presence of these impurities can impact the purity and performance of zeolite, affecting its potential applications in various fields. The primary elemental composition of the CFA-derived zeolite was determined using EDS analysis, as shown in Figure 5C. This analysis revealed that the dominant elements in the zeolite are O, Si, and Al, with weight percentages of 56.4%, 20.9%, and 20.4%, respectively. Notably, the weight percentages of Al and Si in the zeolite molecular sieve are nearly identical, at 20.4% and 20.9%, respectively. When compared to the XRF analysis of pretreated fly ash, the contents of Al and Si did not show a significant decrease through hydrothermal synthesis.

As illustrated in Figures 6A and 6B, the nitrogen adsorption-desorption isotherms of CFA-derived zeolite exhibit a type IV isotherm with an H3 hysteresis loop, in accordance with the classification standards of the International Union of Pure and Applied Chemistry (IUPAC). The larger hysteresis loops at higher relative pressure (P/P0) suggests the presence of abundant mesopores in the zeolite.[36] Distribution of apertures calculated by BJH revealed that the specific surface area of the synthetic CFA-derived zeolite is 17.5 m^2/g, with an average pore size of approximately 10.7 nm and a pore volume of about 0.03 cm^3/g. Consequently, the synthetic zeolite is highly capable of adsorbing NH_3-N, allowing it to freely enter and exit the channels, thereby facilitating efficient mass transfer diffusion. Thermogravimetric analysis (TGA) was employed to evaluate the thermal stability of the zeolite. As shown in Figure 6C, the weight loss of the zeolite can be divided into two steps: before 250°C and between 250°C and 400°C. In the first step, zeolite lost 17.08% of its weight, attributed to the evaporation of free water. Rapid weight loss occurred between 96.6°C and 176.4°C, peaking at 143.5°C. When the temperature rose to 250°C, the rate of weight loss began to decrease, corresponding to the removal of adsorbed and structurally coordinated water, which accounted for an additional 3.2% weight loss. These data indicate that the crystal water in the zeolite constitutes about 20% of its weight. Since the operating temperature for using zeolite to remove NH_3-N from aquaculture wastewater is significantly lower than 400°C, the synthetic zeolite meets the requirements for freshwater pearl farming wastewater treatment.

Optimizing for adsorption parameters of CFA-derived zeolite

Through a series of test, the synthetic zeolite can be confirmed as an A-type zeolite with cubic and spherical crystals microstructure, whose specific surface area of the synthetic CFA-derived zeolite is 17.5 m^2/g, with an average pore size of approximately 10.7 nm and a pore volume of about 0.03 cm^3/g. Moreover, its decomposition temperature is higher than 400°C. Then, the influence of adsorption parameters was further investigated including the adsorption pH, adsorption time, adsorption temperature, initial NH_3-N concentration, and coexisting ions. The removal capacity of NH_3-N is most effective when the pH value ranges from 6 to 8, as shown in Figure 7A. Outside of this range, the removal efficiency declines. At lower pH levels, a high concentration of free protons in the solution causes NH_3-N to primarily convert to NH^{4+}. Because the ionic radius of protons is significantly smaller than that of NH^{4+}, protons more readily occupy the zeolite's internal binding adsorption sites, reducing its ability to adsorb ammonia nitrogen. On the other hand, at higher pH levels, an increased concentration of free OH^- causes ammonia nitrogen to mainly exist as $NH_3 \cdot H_2O$. This decreases the ion exchange efficiency of the zeolite for NH^{4+}, as the adsorption sites become occupied by $NH_3 \cdot H_2O$, leading to a less effective overall adsorption process. The influence of adsorption time and temperature on removal efficiency shows a similar trend (Figures 7B and 7C). The highest removal efficiency occurs at 90 min and 25°C, respectively. Extending the adsorption time or increasing the adsorption temperature does not improve the results.

The adsorption of NH_3-N by zeolite increases with the initial concentration of the NH_3-N solution, though the removal rate declines as the concentration rises (Figure 7D). This is because higher NH_3-N concentrations offer more adsorbates for ion exchange and adsorption. Furthermore, the significant concentration gradient generates a stronger driving force, enabling adsorbates to penetrate deeper into the zeolite and access internal adsorption sites that are less accessible, thus boosting the adsorption capacity. However, when the amount of zeolite remains constant, increasing the initial ammonia nitrogen concentration causes the adsorption capacity of the zeolite to near saturation. Freshwater pearl farming wastewater often contains additional substances such as Na^+ and Ca^{2+}, which may

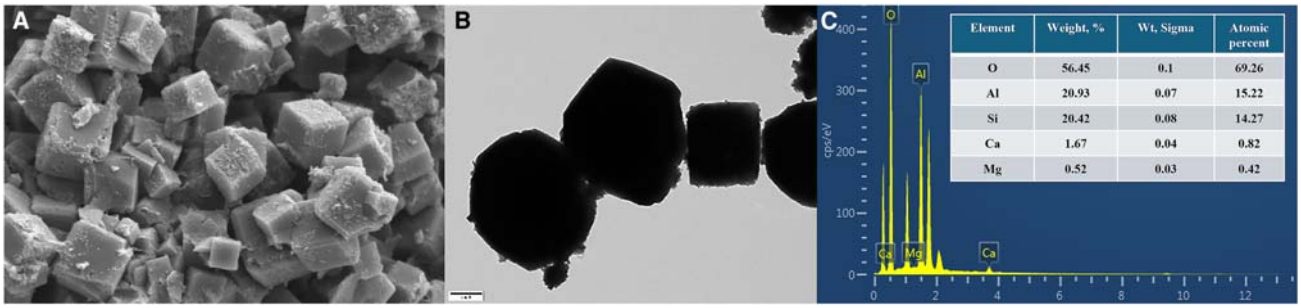

Figure 5. Morphology and component of CFA-derived zeolite
(A) SEM; (B) TEM; (C) EDS.

decrease the ammonium uptake by zeolite.[37] To examine this, the impact of Na^+, Ca^{2+}, K^+, and Mg^{2+} on ammonium adsorption by zeolite was studied (Figure 7E). With an initial ammonium concentration of 100 mg/L, the removal efficiency was 82.3% without any coexisting ions. In the presence of Mg2+, K+, Ca2+, and Na+, the removal efficiencies were 74.9%, 60.5%, 61.7%, and 69.9%, respectively. These results indicate that the presence of cations reduces the ammonium adsorption capacity because they compete with ammonium for available ion exchange sites. The removal efficiency of ammonium was slightly affected by Mg^{2+} and Na^+, but significantly reduced by Ca^{2+} and K^+, likely due to the adsorption affinities of the cations. Mg^{2+} has a lower adsorption affinity, attributed to its smaller ion radius, making it less likely to exchange onto the zeolite

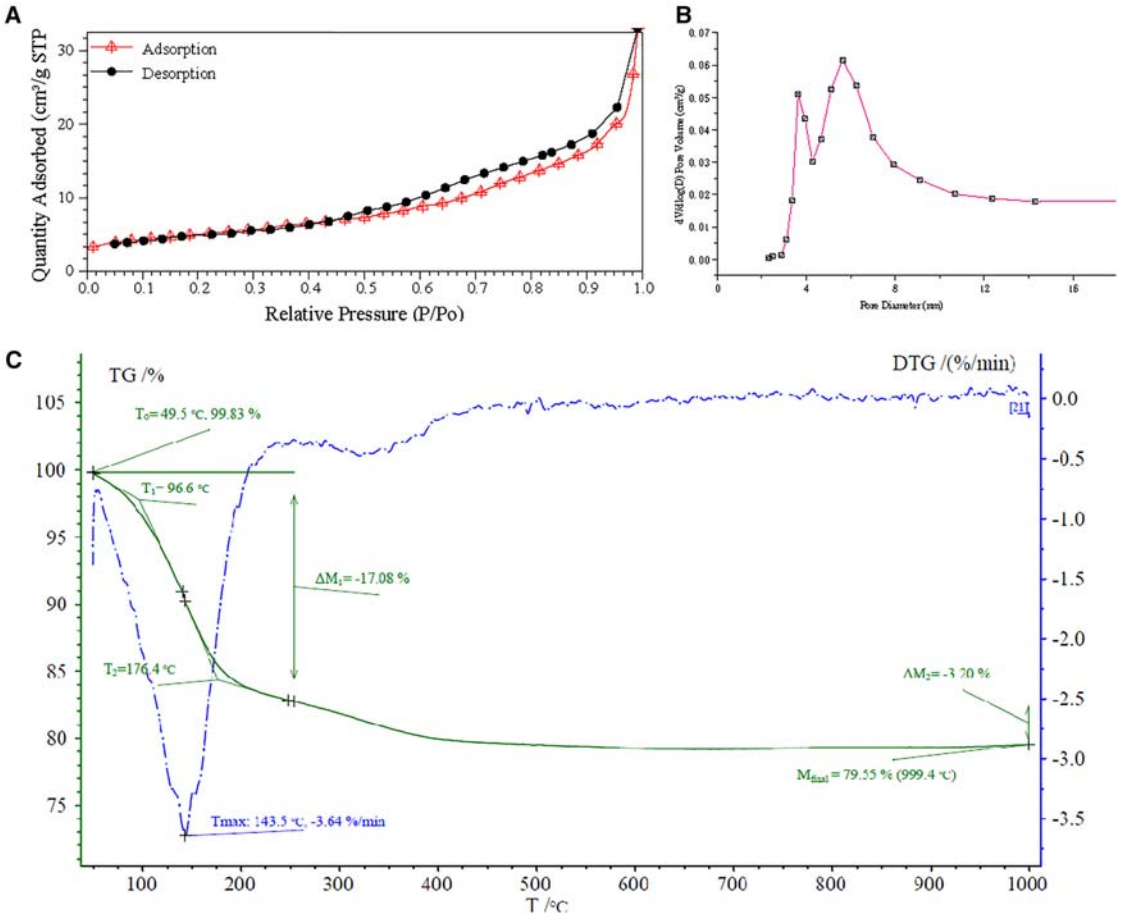

Figure 6. Surface and thermal properties of CFA-derived zeolite
(A) N_2 adsorption and desorption curve; (B) distribution of apertures calculated by BJH; (C) TGA.

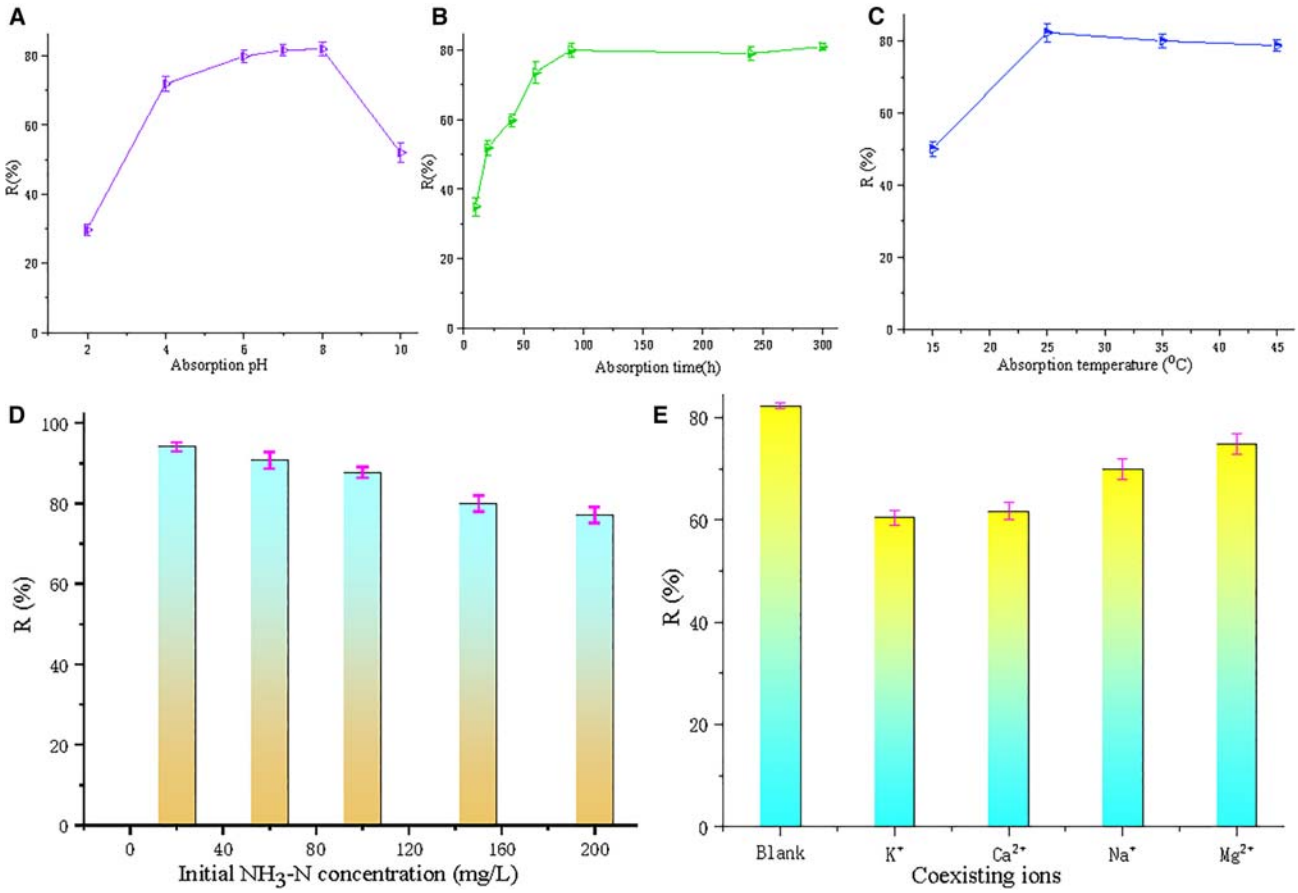

Figure 7. Adsorption parameters optimization of CFA-derived zeolite

Adsorption parameters optimization of CFA-derived zeolite, data are represented as mean ± SEM: (A) pH; (B) time; (C) temperature; (D) initial NH_3-N concentration; (E) coexisting ions.

structure. Despite previous studies indicating the order of ammonium adsorption as $Ca^{2+} > K^+ > Na^+ > Mg^{2+}$,[38] our investigation found that the selectivity order for ammonium over other cations on the synthesized zeolite is $K^+ > Ca^{2+} > Na^+ > Mg^{2+}$.

Adsorption kinetics and adsorption isotherm analyses were conducted to clarify the adsorption characteristics of synthetic CFA-derived zeolite. As shown in Figure 8A, the ammonium adsorption by CFA-derived zeolite was very rapid between 10 and 40 min, primarily dominated by surface adsorption (boundary layer diffusion). From 40 to 90 min, the adsorption rate was mainly driven by intraparticle diffusion, during which NH^{4+} ions moved from the exterior surface of the adsorbent to its pores. In this phase, the mass transfer faced greater resistance, resulting in a decreased adsorption rate. The rapid adsorption of ammonium on CFA-derived zeolite is likely due to the abundance of vacant adsorption sites, with equilibrium typically reached within 90 min.[39] Figure 8A also demonstrates the application of pseudo-first-order, pseudo-second-order, Bangham, and Elovich models to explain the adsorption kinetics of the synthetic zeolite. The fitting correlation coefficient (R^2) for the Elovich model is 0.73, in contrast, the quasi-first-order model has the highest fitting correlation coefficient, with an R^2 of 0.98. This suggests that the quasi-first-order model more accurately represents the kinetics and effect of CFA-derived zeolite in the ammonia nitrogen adsorption process compared to the Elovich model. The adsorption isotherm analyses of CFA-derived zeolite are presented in Figure 8B. The correlation coefficients (R^2) for the Langmuir, Freundlich, Temkin, and D-R models were 0.97, 0.91, 0.92, and 0.99, respectively. The Dubinin-Radushkevich best represents the adsorption behavior of fly ash zeolite molecular sieves on ammonia nitrogen in simulated wastewater, indicating that the adsorption primarily involves microporous ion adsorption. The b_T value in the Temkin model is higher than 1, suggesting the presence of some degree of chemisorption. Given that the R^2 of the D-R model is greater than that of the Temkin model, it can be inferred that the adsorption process is mainly driven by ion exchange, with chemisorption playing a supporting role.

Dealing with actual freshwater pearl farming wastewater

After a series of determinations, we have demonstrated that CFA-derived zeolite possesses a high NH_3-N removal capacity, ultimately proving effective in practical applications. To the best of our knowledge, the raw wastewater from freshwater pearl

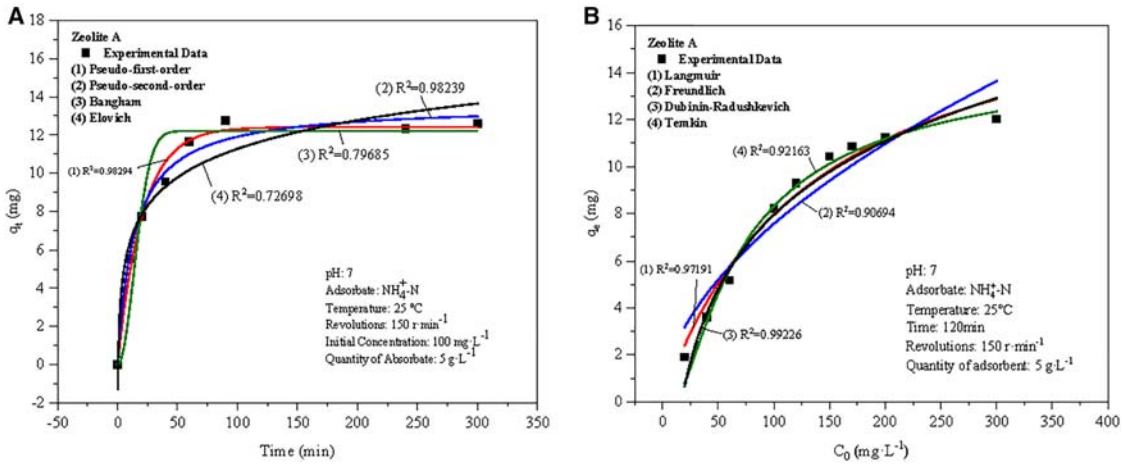

Figure 8. Adsorption kinetics isotherm analyses of CFA-derived zeolite
(A) adsorption kinetics and (B) adsorption isotherm analyses.

farming poses a significant threat to the local environment, yet it has not received substantial attention from researchers. Very few studies have focused on addressing the challenges associated with raw freshwater pearl farming wastewater. We hope this study will provide a valuable starting point. This study specifically examined whether CFA-derived zeolite could significantly remove NH_3-N from raw freshwater pearl farming wastewater, which was treated solely by solid/liquid separation. The results of using synthetic CFA-derived zeolite to remove NH_3-N from raw freshwater pearl farming wastewater are listed in Table 1. These results indicate that the synthetic zeolite is indeed effective at removing NH_3-N from raw freshwater pearl farming wastewater. The highest removal efficiency reached 74% at a zeolite dosage of 70 g/L. However, this efficiency is notably lower than the 94% removal observed in optimized adsorption conditions. This decrease in efficiency may be attributable to the presence of P, K, and other particulates that could interfere with NH_3-N adsorption. Despite the inhibitory effects of some coexisting cations in the raw wastewater, it is undeniable that CFA-derived zeolite demonstrates good efficiency in the removal of ammonium from raw freshwater pearl farming wastewater.

Table 1. Results of synthetic CFA-derived zeolite removal NH_3-N from raw freshwater pearl farming wastewater

Entry	Dosage of zeolite (g/L)	Removal efficiency (%)[a,b]
1	10	21.5
2	20	47.7
3	30	53.2
4	40	60.4
5	50	68.9
6	60	72.3
7	70	74.2

[a]Adsorption conditions: pH = 7.5, 25.°C, 120 min.
[b]measured using Nessler's reagent spectrophotometry, and three replicates were performed in parallel for each set of experiments.

Conclusions

In summary, this study demonstrated a synthesis route for CFA-derived zeolite, which exhibited good adsorption efficiency for raw freshwater pearl farming wastewater. The CFA-derived zeolite was prepared using both pickling pretreatment and hydrothermal synthesis methods. Through XRD, BET, SEM, TEM, and TGA tests, the synthetic zeolite was confirmed to be an A-type zeolite with cubic and spherical crystal microstructures. The specific surface area of the synthetic CFA-derived zeolite was found to be 17.5 m^2/g, with an average pore size of approximately 10.7 nm and a pore volume of about 0.03 cm^3/g. Additionally, TG analysis results indicate that the synthetic zeolite could be safe when the adsorption temperature is lower than 100°C. The adsorption process of NH_3-N was also thoroughly investigated. Adsorption kinetics and isotherm analyses indicated that the pseudo-first-order and Dubinin-Radushkevich models more accurately represent the kinetics and adsorption behavior of CFA-derived zeolite in the NH_3-N adsorption process. When used to remove NH_3-N from raw freshwater pearl farming wastewater, the removal efficiency reached 74% at a dosage of 70 g/L. Given the ease of acquiring CFA-derived zeolite, this study provides a valuable starting point for addressing freshwater pearl farming wastewater treatment.

Limitations of the study

Despite demonstrating a viable synthesis route for CFA-derived A-type zeolite with good adsorption efficiency for NH_3-N removal, this study has several limitations.

First, achieving a removal efficiency of 74% requires a relatively high zeolite dosage of 70 g/L, which may not be economically feasible for large-scale applications; optimization of dosage and process conditions is necessary for practical implementation.

Second, the study focused solely on NH_3-N removal without considering other potential contaminants present in freshwater pearl farming wastewater that could interfere with the adsorption process.

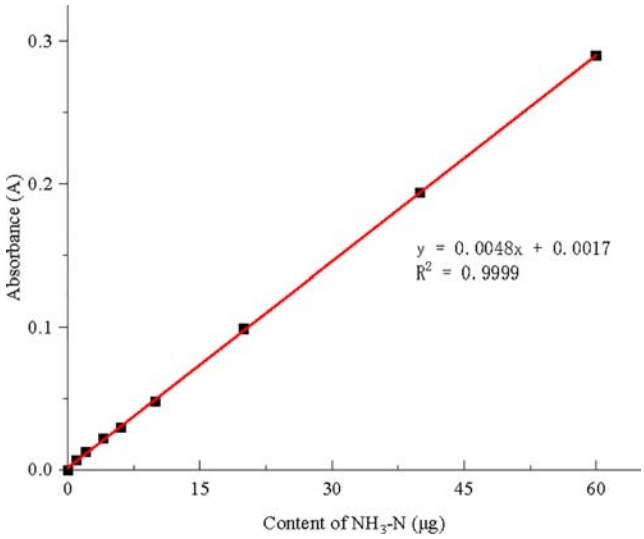

Figure 9. Standard curve Nessler's reagent spectrophotometry

Third, the long-term stability and reusability of the CFA-derived zeolite were not evaluated, leaving questions about the sustainability and cost-effectiveness of the treatment over time.

Additionally, while adsorption kinetics and isotherm models were analyzed, the mechanisms at a molecular level were not explored, which could provide deeper insights into improving the adsorption capacity. Future research should address these limitations by optimizing operational parameters, evaluating the treatment of mixed contaminants, assessing the reusability of zeolite, and investigating the adsorption mechanisms in more detail.

RESOURCE AVAILABILITY

Lead contact

Further information and requests for resources and reagents should be directed to and will be fulfilled by the lead contact, Bo Xia (11106142@zju.edu.cn).

Materials availability

This study did not generate new unique reagents.

Data and code availability

- All data reported in this paper will be available from the lead contact upon request.
- This article does not report new datasets of a standardized datatype.
- Any additional information required to reanalyze the data reported in this paper is available from the lead contact upon request.

ACKNOWLEDGMENTS

Research Foundation of Jiyang College of Zhejiang A&F University (RC2023S02).

AUTHOR CONTRIBUTIONS

X.B. supervised this project and wrote the manuscript; C.H. preparing zeolite, investigated the pretreatment and hydrothermal Synthesis; W.J., optimizing the adsorption process; P.X. characterization of the synthetic zeolite and searching for founding.

DECLARATION OF INTERESTS

The authors declare no competing interests.

STAR★METHODS

Detailed methods are provided in the online version of this paper and include the following:

- KEY RESOURCES TABLE
- EXPERIMENTAL MODEL AND STUDY PARTICIPANT DETAILS
  - Preparation of CFA-derived zeolite
  - Adsorption experiments
  - X-Ray fluorescence (XRF) analysis
  - X-Ray diffraction (XRD) analysis
  - Transmission electron microscope (TEM) analysis
  - Brunauer-Emmett-Teller (BET) analysis
  - Scanning electron microscopy (SEM) and energy dispersive spectrometer (EDS) analysis
- QUANTIFICATION AND STATISTICAL ANALYSIS

Received: July 23, 2024
Revised: October 17, 2024
Accepted: December 17, 2024
Published: December 19, 2024

REFERENCES

1. Wang, J., Zhou, W., Chen, H., Zhan, J., He, C., and Wang, Q. (2018). Ammonium nitrogen tolerant chlorella strain screening and its damaging effects on photosynthesis. Front. Microbiol. *9*, 3250. https://doi.org/10.3389/fmicb.2018.03250.
2. Zhu, K., Fu, H., Zhang, J., Lv, X., Tang, J., and Xu, X. (2012). Studies on removal of NH4+-N from aqueous solution by using the activated carbons derived from rice husk. Biomass Bioenergy *43*, 18–25. https://doi.org/10.1016/j.biombioe.2012.04.005.
3. Beckinghausen, A., Odlare, M., Thorin, E., and Schwede, S. (2020). From removal to recovery: an evaluation of nitrogen recovery techniques from wastewater. Appl. Energy *263*, 114616. https://doi.org/10.1016/j.apenergy.2020.114616.
4. Tang, H., Xu, X., Wang, B., Lv, C., and Shi, D. (2020). Removal of Ammonium from Swine Wastewatern Using Synthesized Zeolite from Fly Ash. Sustainability *12*, 3423. https://doi.org/10.3390/su12083423.
5. An, Q., Li, Z., Zhou, Y., Meng, F., Zhao, B., Miao, Y., and Deng, S. (2021). Ammonium removal from groundwater using peanut shell based modified biochar: mechanism analysis and column experiments. Journal of Water Process Engineering *43*, 102219. https://doi.org/10.1016/j.jwpe.2021.102219.
6. Beckinghausen, A., Reynders, J., Merckel, R., Wu, Y.W., Marais, H., and Schwede, S. (2020). Postpyrolysis treatments of biochars from sewage sludge and A. mearnsii for ammonia (NH4-n) recovery. Appl. Energy *271*, 115212. https://doi.org/10.1016/j.apenergy.2020.115212.
7. Feng, Y., Hu, T., Wu, M., Shangguan, J., Fan, H., and Mi, J. (2016). Effect of microwave irradiation on the preparation of iron oxide/arenaceous clay sorbent for hot coal gas desulfurization. Fuel Process. Technol. *148*, 35–42. https://doi.org/10.1016/j.fuproc.2016.01.037.
8. Feng, Y., Wen, J., Hu, Y., Wu, B., Wu, M., and Mi, J. (2017). Evaluation of the cycling performance of a sorbent for H2S removal and simulation of desulfurization-regeneration processes. Chem. Eng. J. *326*, 1255–1265. https://doi.org/10.1016/j.cej.2017.05.098.
9. Feng, Y., Wang, J., Hu, Y., Lu, J., Zhang, M., and Mi, J. (2020). Microwave heating motivated performance promotion and kinetic study of iron oxide sorbent for coal gas desulfurization. Fuel *267*, 117215. https://doi.org/10.1016/j.fuel.2020.117215.

10. Sun, Y., Zhang, X., Zhang, M., Ge, M., Wang, J., Tang, Y., Zhang, Y., Mi, J., Cai, W., Lai, Y., and Feng, Y. (2022). Rational design of electrospun nanofibers for gas purification: Principles, opportunities, and challenges. Chem. Eng. J. *446*, 137099. https://doi.org/10.1016/j.cej.2022.137099.

11. Zhang, X., Ru, Z., Wang, T., Feng, W., Zhang, M., Wang, J., Mi, J., Ge, M., and Feng, Y. (2023). Insights to the microwave effect in formation and performance promotion of iron-based carbon nanofibrous composites for H_2S removal. Compos. Commun. *37*, 101468. https://doi.org/10.1016/j.coco.2022.101468.

12. Zhang, X., Ru, Z., Sun, Y., Zhang, M., Wang, J., Ge, M., Liu, H., Wu, S., Cao, C., Ren, X., et al. (2022). Recent advances in applications for air pollutants purification and perspectives of electrospun nanofibers. J. Clean. Prod. *378*, 134567. https://doi.org/10.1016/j.jclepro.2022.134567.

13. Ru, Z., Zhang, X., Zhang, M., Mi, J., Cao, C., Yan, Z., Ge, M., Liu, H., Wang, J., Zhang, W., et al. (2022). Bimetallic-MOF-Derived $Zn_xCo_{3-x}O_4$/Carbon Nanofiber Composited Sorbents for High-Temperature Coal Gas Desulfurization. Environ. Sci. Technol. *56*, 17288–17297. https://doi.org/10.1021/acs.est.2c04193.

14. Feng, Y., Zhang, M., Sun, Y., Cao, C., Wang, J., Ge, M., Cai, W., Mi, J., and Lai, Y. (2023). Porous carbon nanofibers supported Zn@MnO_x sorbents with high dispersion and loading content for hot coal gas desulfurization. Chem. Eng. J. *464*, 142590. https://doi.org/10.1016/j.cej.2023.142590.

15. Feng, W., Zhang, M., Zhang, X., Mi, J., Yang, C., Wang, J., and Feng, Y. (2024). Carbon nanofibers supported sorbents with enhanced performance via microwave-assisted in-situ structural modifications for H_2S removal. Separation and Purification Technology *350*, 127883. https://doi.org/10.1016/j.seppur.2024.127883.

16. Wu, Y., Liang, G., Zhao, X., Wang, H., and Qu, Z. (2023). Flexible textural design of ZSM-5 zeolite adsorbent from coal fly ash via solvent-free method for toluene elimination. J. Environ. Chem. Eng. *11*, 109589. https://doi.org/10.1016/j.jece.2023.109589.

17. Zhang, K., Van Dyk, L., He, D., Deng, J., Liu, S., and Zhao, H. (2021). Synthesis of zeolite from fly ash and its adsorption of phosphorus in wastewater. Green Process. Synth. *10*, 349–360. https://doi.org/10.1515/gps-2021-0032.

18. El Bojaddayni, I., Emin Küçük, M., El Ouardi, Y., Jilal, I., El Barkany, S., Moradi, K., Repo, E., Laatikainen, K., and Ouammou, A. (2023). A review on synthesis of zeolites from natural clay resources and waste ash: Recent approaches and progress. Miner. Eng. *198*, 108086. https://doi.org/10.1016/j.mineng.2023.108086.

19. Lin, Y.J., and Chen, J.C. (2021). Resourcization and valorization of waste incineration fly ash for the synthesis of zeolite and applications. J. Environ. Chem. Eng. *9*, 106549. https://doi.org/10.1016/j.jece.2021.106549.

20. Liu, Z., Li, S., Li, L., Wang, J., Zhou, Y., and Wang, D. (2019). One-step high efficiency crystallization of zeolite A from ultra-fine circulating fluidized bed fly ash by hydrothermal synthesis method. Fuel *257*, 116043. https://doi.org/10.1016/j.fuel.2019.116043.

21. Murakami, T., Otsuka, K., Fukasawa, T., Ishigami, T., and Fukui, K. (2023). Hierarchical porous zeolite synthesis from coal fly ash via microwave heating. Colloids Surf. A Physicochem. Eng. Asp. *661*, 130941. https://doi.org/10.1016/j.colsurfa.2023.130941.

22. Zeng, X., Hu, X., Song, H., Xia, G., Shen, Z.Y., Yu, R., and Moskovits, M. (2021). Microwave synthesis of zeolites and their related applications. Microporous Mesoporous Mater. *323*, 111262. https://doi.org/10.1016/j.micromeso.2021.111262.

23. Kim, M.I., Im, J.S., Seo, S.W., Cho, J.H., Lee, Y.S., and Kim, S. (2020). Preparation of pitch-based activated carbon with surface-treated fly ash for SO2 gas removal. Carbon Lett *30*, 381–387. https://doi.org/10.1007/s42823-019-00107-y.

24. He, P., Qin, H., Zhang, Y., Zhao, X., Chen, N., and Wu, J. (2020). Influence of mercury retention on mercury adsorption of fly ash. Energy *204*, 117927. https://doi.org/10.1016/j.energy.2020.117927.

25. Li, Z., Qian, W., Chen, Y., Xu, P., Li, J., and Yang, J. (2021). A new treasure in industrial solid waste—coal fly ash for effective oil/water separation. J. Taiwan Inst. Chem. Eng. *118*, 196–203. https://doi.org/10.1016/j.jtice.2020.12.026.

26. Oliveira, J.A., Cunha, F.A., and Ruotolo, L.A. (2019). Synthesis of zeolite from sugarcane bagasse fly ash and its application as a low-cost adsorbent to remove heavy metals. J. Clean. Prod. *229*, 956–963. https://doi.org/10.1016/j.jclepro.2019.05.069.

27. Ye, C., Yan, B., Ji, X., Liao, B., Gong, R., Pei, X., and Liu, G. (2019). Adsorption of fluoride from aqueous solution by fly ash cenospheres modified with paper mill lime mud: Experimental and modeling. Ecotoxicol. Environ. Saf. *180*, 366–373. https://doi.org/10.1016/j.ecoenv.2019.04.086.

28. Xu, R., Lyu, T., Wang, L., Yuan, Y., Zhang, M., Cooper, M., Mortimer, R.J.G., Yang, Q., and Pan, G. (2022). Utilization of coal fly ash waste for effective recapture of phosphorus from waters. Chemosphere *287*, 132431. https://doi.org/10.1016/j.chemosphere.2021.132431.

29. Meng, R., Lv, P., Yang, Y., Xu, D., Gao, T., and Fu, Y. (2020). Low-temperature alkali-modified fly ash as an effective adsorbent for removal of ammonia nitrogen, phosphorus and COD from the wastewater. Earth and Environmental Science *569*, 012026. https://doi.org/10.1088/1755-1315/569/1/012026.

30. Juan, R., Hernández, S., Andrés, J.M., and Ruiz, C. (2007). Synthesis of granular zeolitic materials with high cation exchange capacity from agglomerated coal fly ash. Fuel *86*, 1811–1821. https://doi.org/10.1016/j.fuel.2007.01.011.

31. Ren, X.Y. (2020). Synthesis, Growth Mechanism and Adsorption Performance of Zeolites Based on Coal Fly Ash. Doctoral dissertation.

32. Ojumu, T.V., Du Plessis, P.W., and Petrik, L.F. (2016). Synthesis of zeolite A from coal fly ash using ultrasonic treatment–A replacement for fusion step. Ultrason. Sonochem. *31*, 342–349. https://doi.org/10.1016/j.ultsonch.2016.01.016.

33. Ren, X., Xiao, L., Qu, R., Liu, S., Ye, D., Song, H., Wu, W., Zheng, C., Wu, X., and Gao, X. (2018). Synthesis and characterization of a single-phase zeolite A using coal fly ash. RSC Adv. *8*, 42200–42209. https://doi.org/10.1088/2053-1591/aac3ae.

34. Serati-Nouri, H., Jafari, A., Roshangar, L., Dadashpour, M., Soltanahmadi, Y.P., and Zarghami, N. (2020). Biomedical applications of zeolite-based materials: A review. Mater. Sci. Eng. C *116*, 111225. https://doi.org/10.1016/j.msec.2020.111225.

35. Cardoso, A.M., Paprocki, A., Ferret, L.S., Azevedo, C.M., and Pires, M. (2015). Synthesis of zeolite Na-P1 under mild conditions using Brazilian coal fly ash and its application in wastewater treatment. Fuel *139*, 59–67. https://doi.org/10.1016/j.fuel.2014.08.016.

36. Liu, Y., Wang, G., Luo, Q., Li, X., and Wang, Z. (2018). The thermodynamics and kinetics for the removal of copper and nickel ions by the zeolite Y synthesized from fly ash. Mater. Res. Express *6*, 025001. https://doi.org/10.1088/2053-1591/aaea41.

37. Kizito, S., Wu, S., Kipkemoi Kirui, W., Lei, M., Lu, Q., Bah, H., and Dong, R. (2015). Evaluation of slow pyrolyzed wood and rice husks biochar for adsorption of ammonium nitrogen from piggery manure anaerobic digestate slurry. Sci. Total Environ. *505*, 102–112. https://doi.org/10.1016/j.scitotenv.2014.09.096.

38. Weatherley, L.R., and Miladinovic, N.D. (2004). Comparison of the ion exchange uptake of ammonium ion onto New Zealand clinoptilolite and mordenite. Water Res. *38*, 4305–4312. https://doi.org/10.1016/j.watres.2004.08.026.

39. Lin, L., Lei, Z., Wang, L., Liu, X., Zhang, Y., Wan, C., Lee, D.-J., and Tay, J.H. (2013). Adsorption mechanisms of high-levels of ammonium onto natural and NaCl-modified zeolites. Sep. Purif. Technol. *103*, 15–20. https://doi.org/10.1016/j.seppur.2012.10.005.

STAR★METHODS

KEY RESOURCES TABLE

REAGENT or RESOURCE	SOURCE	IDENTIFIER
Coal fly ash	Local thermal power plant in Zhejiang	-
$Al(OH)_3$	Energy Chemical Ltd.	Cat# 21645-51-2
NaOH	Energy Chemical Ltd.	Cat# 1310-73-2
hydrochloric acid	Energy Chemical Ltd.	Cat# 7647-01-0

EXPERIMENTAL MODEL AND STUDY PARTICIPANT DETAILS

Preparation of CFA-derived zeolite

Pretreatment of CFA

After the CFA was passed through standard sample sieves of various mesh sizes, 1.0 g of CFA was placed into a 100 mL round-bottom flask. A specific volume and concentration of hydrochloric acid were then added. A condensation return device was installed on the flask, which was then placed in a constant temperature oil bath. The mixture was stirring at a set temperature for a predetermined time. After cooling, the mixture was filtered, and the resulting cake was washed several times with deionized water until the pH value was close to 7.0. The cake was then dried at 105°C for 24 h, ground, and screened using a 200-mesh standard sample sieve. X-ray fluorescence (XRF) was used to measure the elemental content of the CFA post-pickling.

Hydrothermal zeolite synthesis

1.0 g of acid-leached CFA was transferred into a mortar. The required mass of $Al(OH)_3$ was then calculated and weighed based on a Si/Al mole ratio of 1. Subsequently, NaOH was added to adjust the alkali-to-ash mass ratio between 0.5 and 1.5. The mixture was calcined at 750°C for 2 h and then ground after cooling. Next, this 1.0 g alkali-melted product was combined with a specific amount of deionized water, and the mixture underwent a hydrothermal reaction at a specified temperature. After the reaction, the product was cooled, centrifuged, and washed until the pH was between 9 and 10. Finally, the product was dried at 105°C for 12 h, and the CFA-derived zeolite was obtained after grinding.

Adsorption experiments

The removal rate and adsorption capacity of NH_3-N from simulated wastewater by CFA-derived zeolite were determined by Nesser's reagent spectrophotometry. The removal efficiency (R) and the adsorption capacities of adsorbents at time (q_t, mg/g) and at equilibrium (q_e, mg/g) were calculated using the following equations:

$$R = \frac{(C_0 - C_t)}{C_0} \times 100\ \%$$

$$qt = \frac{(C_0 - C_t)V}{m}$$

$$q_e = \frac{(C_0 - C_e)V}{C_0}$$

where q_e (mg/g) is the equilibrium adsorption capacity of NH_3-N; C_0, Ct, and C_e (mg/mL) are the NH_3-N concentrations at the start, any time (t), and equilibrium, respectively; V is the total solution volume (L); and m is the mass of the adsorbents (g).

The standard curve was established using NH_3-N standard solutions. Standard solutions containing 0.0 μg, 1.0 μg, 2.0 μg, 4.0 μg, 6.0 μg, 10.0 μg, 20.0 μg, 40.0 μg, and 60.0 μg of NH_3-N were prepared in 25.0 mL volumes. To each solution, 1.0 mL of a 500 mg/L potassium and sodium tartrate solution was added, followed by the addition of 1.0 mL of Nessler's reagent, and the mixtures were thoroughly mixed. After calibrating at zero point, the ultraviolet spectrophotometer was preheated for 30 min. The absorbance was measured at a scanning wavelength of 450 nm, using water as the reference. The absorbance of the blank solution was subtracted from each measurement to obtain the corrected absorbance values, which were averaged over three determinations. The standard curve is illustrated in Figure 9, with the equation of the curve being y = 0.0048x+0.0017.

After establishing the standard curve, the adsorption capacity of the CFA-derived zeolite was investigated. Batch experiments were conducted using 250 mL Erlenmeyer flasks, each containing 100 mL of a 100 mg/L NH_3-N solution and 1.0 g of CFA-derived zeolite. The flasks were sealed and shaken at 180 rpm for 2 h on a mechanical shaker at a specified temperature. The NH_3-N content of the final reaction mixtures was determined using the established standard curve procedures and calculated with the corrected

standard curve fitting equation. The removal rate of ammonia nitrogen and the adsorption capacity of NH_3-N by the zeolite were then calculated based on this equation. The influence factors on NH_3-N adsorption were studied by varying pH (2–10), initial NH_3-N concentration (20–200 mg/L), adsorption time (10–300 min), and adsorption temperature (15°C–45°C). Additionally, the effect of coexisting ions (Na^+, Ca^{2+}, K^+, Mg^{2+}) on ammonium adsorption was investigated at individual ion concentrations of 0.01 M.

X-Ray fluorescence (XRF) analysis

XRF was used for the multielement analysis of the CFA samples (Philips PW2404, Philips Co. Holland). The tests were performed in triplicate, and their average data were reported.

X-Ray diffraction (XRD) analysis

The XRD used for detection was the Rigaku Ultima IV from Japan. The instrument employed a copper target tube with a K-α diffraction source, operating at a tube voltage of 40 kV and a tube current of 40 mA. The scanning rate was set to 8° per minute, covering an angle range from 5° to 60°.

Transmission electron microscope (TEM) analysis

TEM images were tested using JEOL JEM 2100F operating at 200 kV. The samples for TEM characterization were prepared by placing and evaporating a drop of the sample in ethanol on carbon-coated gold grid.

Brunauer-Emmett-Teller (BET) analysis

The specific surface area and pore size distribution of the catalyst were determined using the Brunauer-Emmett-Teller (BET) method, employing the advanced ASAP 2460 Version 3.01 instrument from MAC as the testing platform. Nitrogen was used as the adsorbent, and the test was conducted at a temperature of 77.300K.

Scanning electron microscopy (SEM) and energy dispersive spectrometer (EDS) analysis

Using the German ZEISS Sigma 300 scanning electron microscope, the probe area is 60 mm^2, the thermal field emission electron source, the acceleration voltage is 5.0 kV, the magnification is 20–100,000 times, the elemental analysis range of the X-ray spectrometer is: Be4-Am95.

QUANTIFICATION AND STATISTICAL ANALYSIS

The Microsoft Excel 365 function LINEST was used to perform the regression from the measured adsorption kinetics isotherm (Figure 8) and standard curve Nesser's reagent (Figure 9). The Microsoft Excel 365 functions STDEV, COUNT and SQRT were used to perform the standard error of the mean (SEM) (Figures 2, 3, and 7).